International Journal of Biological Macromolecules 178 (2021) 464–476

Contents lists available at ScienceDirect

International Journal of Biological Macromolecules

journal homepage: http://www.elsevier.com/locate/ijbiomac

Physicochemical characterization, drug release, and biocompatibility evaluation of carboxymethyl cellulose-based hydrogels reinforced with sepiolite nanoclay

Ramasubba Reddy Palem [a], Kummara Madhusudana Rao [b], Ganesh Shimoga [c], Rijuta G. Saratale [d], Surendra K. Shinde [e], Gajanan S. Ghodake [e], Soo-Hong Lee [a,*]

[a] Department of Medical Biotechnology, Biomedical Campus 32, Gyeonggi 10326, Republic of Korea
[b] School of Chemical Engineering, Yeungnam University, 280 Daehak-Ro, Gyeongsan 38541, Republic of Korea
[c] Advanced Technology Research Center, Future Convergence Engineering, Korea University of Technology and Education, Cheonan-si, Chungcheongnam-do 330-708, Republic of Korea
[d] Research Institute of Biotechnology and Medical Converged Science, Dongguk University-Seoul, Ilsandong-gu, Goyang-si, Gyeonggi-do, Seoul 10326, Republic of Korea
[e] Department of Biological and Environmental Science, Dongguk University-Seoul, Ilsandong-gu, Goyang-si, Gyonggido, Seoul 10326, Republic of Korea

ARTICLE INFO

Article history:
Received 8 February 2021
Received in revised form 19 February 2021
Accepted 25 February 2021
Available online 1 March 2021

Keywords:
Caboxymethyl cellulose
Polymer-clay hydrogels
Physico-chemical properties
Drug release
In-vitro cytocompatibility

ABSTRACT

Polymer–clay nanocomposite hydrogel films (PCNCHFs) were prepared from caboxymethyl cellulose, polyvinylpyrrolidone, agar and nanosepiolite clay (0, 0.3, 0.5, 0.7, 0.9 and 1.5% reinforcement) by treating thermally in a simple, rapid, and inexpensive route. The PCNCHFs and its 5-fluorouracil (FU)-loaded composites (PCNCHFs@FU) were tested for FU release and characterized by FTIR, XRD, FE-SEM, EDX, DSC, and TGA analyses to investigate their structural, morphological, and thermal properties. The nanosepiolite-loaded polymer composites (PCNCHF1 to PCNCHF5) exhibited higher tensile strength than the pristine polymer hydrogel (PCNCHF0); consequently, the thermal properties (glass- and melting-transition) were improved. The PCNCHFs@FU demonstrated prolonged FU release at pH 7.4 for 32 h. The biocompatibility of PCNCHFs was tested against human skin fibroblast (CCDK) cells. The viability of cells exposed to all PCNCHFs was >95% after 72 h of culture. The live/dead assay show the proliferation of fibroblast cells, confirming the biocompatibility of the hydrogels. The pH-sensitive PCNCHFs@FU release could be suitable for drug release in cancer therapy, and the developed PCNCHFs may also be useful for tissue engineering, food packaging, and other biological applications.

1. Introduction

Biopolymer-based composite hydrogels are in great demand for various applications, including those encompassing the pharmaceutical, environmental, and biomedical fields, due to their economic, environment-friendly, biodegradable, and biocompatible nature [1–3]. In brief, three-dimensional hydrophilic polymeric networks with high water affinity usually do the construction of polymer-based hydrogels. Instead of dissolving into solution, their physically and/or chemically cross-linked structures allow them to hold water [4–6]. Hydrogels can be constituted with different macromolecules with various functional groups, such as -OH, -SO_3H, -COOH, -CONH-, and -$CONH_2$, in their polymeric backbone (either embedded in or grafted to). Because of their hydrophilic functional domains, the resulting hydrogels can absorb and retain large amount of water and other biological fluids/cells. Therefore, these swollen three-dimensional viscoelastic polymer network structures can resemble natural tissue and is of great importance in biomedical field [7–9]. Carboxymethyl cellulose (CMC) based hydrogel systems were developed by different methods, such as physical blending, chemical grafting, and ionic gelation etc. However, the polyelectrolyte behavior of CMC is due to the presence of carboxylate moiety, which is a pH sensitive group with in-situ gelation ability, resulting in bio-adhesive behavior. Hence, the electrically controlled CMC based systems are very useful in delivering various pharmaceuticals such as 5-fluorouracil (FU) for colon drug release, wound dressing, and tissue engineering, because of its biocompatibility [10–16].

Recently, the European Food Safety Authority reported that, CMC is a safe food additive for all animals; moreover, it was also shown to be harmless to the environment because of its biodegradation propensity [17]. The unique viscosity characteristics, hydrophilic nature, adhesive behavior, film forming ability, and biocompatibility, the CMC-based hydrogels have wide range of industrial applications [18–21], in addition to biomedical [22–24] and environmental applications [25–27]. The pristine polymer hydrogels show lower mechanical stability without chemical crosslinking agents. Therefore, it is necessary to use ecofriendly materials as alternative for reinforcement strategy. To

* Corresponding author.
E-mail address: soohong@dongguk.edu (S.-H. Lee).

https://doi.org/10.1016/j.ijbiomac.2021.02.195
0141-8130/

improve the polymer properties, the use of naturally occurring nanoclay materials in reinforcement technique could serve the purpose and is recently gaining much attention. With the increasing focus on the ecological impact, cost effectiveness, and materials safety, naturally available nano-clays (particularly sepiolite), are potentially appealing toward industrial, biomedical, and technological applications [28]. Sepiolite is an inexpensive, abundant, and biocompatible nanofibrous mineral with molecular formula of $Mg_8Si_{12}O_{30}(OH)_4(OH_2)_4.8H_2O$. This Mg-rich silicate material has gained attention for use in various modern industrial sectors due to its fibrous morphology, high surface area, and surface active silanol function groups. Additionally, sepiolite shows excellent adsorption, reinforcing, and bacterial inhibition abilities and carrier properties [28–30], making it useful for the fabrication of a wide range of advanced nanostructured materials. Drug release from a polymer hydrogel can be controlled by reinforcement of the network with appropriate nano-clay additives. However, the incorporation of nano-clay in the polymer hydrogel network can also affect overall physical, chemical, and mechanical properties. This physical and chemical property alteration of nano-clay embedded polymeric hydrogels are significant in consideration for specific applications. Therefore, nano-clay embedded polymer hydrogel networks can tune the swelling properties, thermal withstandability, and mechanical strength of the reinforced hydrogel [31,32].

Most of the existing works on polymer nanocomposites are related to the incorporation of layered silicates of sepiolite into biopolymers like cellulose, starch, gelatin, alginate, chitosan, and polylactides [33–37]. Previous studies have indicated that incorporation of nanofibrous sepiolite into aforementioned polymers can confer fascinating reinforcement characteristics with unique mechanical robustness. Though sepiolite does not primarily exhibit intercalation properties, the natural magnesium silicates (Mg—Si) show notably low porosity and high surface area (i.e., 320 m^2/g for sepiolite) [28,38]. Additionally, the silanol groups (Si–OH) in the nanoclay, which are formed at the discontinuous edge of the silica sheets, interact well with the prepared polymer networks to form homogeneous nanocomposites. This synergistic interaction among inorganic nanoparticles and the functional groups of organic polymers can yield hybrid polymer–clay nanocomposite materials with improved mechanical and thermal properties [39,40].

In the present study, polymer–clay nanocomposite hydrogel films (PCNCHFs) were studied with respect to their structural and morphological characteristics, swelling studies, thermal stability, and mechanical properties. We also examined FU drug release from PCNCHFs and evaluated their cytotoxicity and cytocompatability against fibroblast CCDK cells.

2. Materials and methods

2.1. Materials

Caboxymethyl cellulose sodium (CMC, Mw = 250,000, CAS: 9004-32-4), polyvinylpyrrolidone (PVP, Mw = 40,000, CAS: 9003-39-8), and sepiolite (CAS: 63800–37-3) were procured from Sigma-Aldrich chemicals. Laboratory-grade supplies of the other required chemicals were procured and utilized without any pre-treatment. Additionally, deionized water (DW) was obtained from a water purification system and used in all experiments.

2.2. Preparation of PCNCHFs

The PCNCHFs were prepared in a single step by thermal treatment followed by a casting process [41]. Briefly, polymer–clay solutions (CMC, PVP, and sepiolite) were prepared in sealed glass bottles containing 150 mL of deionized water under 120 °C temperature and 15-lb pressure (107 kPa) for 15 min. The resulting homogeneous polymer–sepiolite solutions were transferred into a clean glass plate (25 × 25 mm diameter) and allowed to cool at ambient conditions. After 24 h, the formed PCNCHFs (0.7–0.9 mm thickness) were soaked in DW to eliminate any surface adherents and soluble impurities and then air dried at approximately 25 °C for one day. The polymer concentration was maintained constant along with small amounts of agar, polyethylene glycol, and glycerin; however, the concentration of the nano-clay, sepiolite (i.e., 180 nm, Fig. S1) was changed to 0%, 0.3%, 0.5%, 0.7%, 0.9%, and 1.5%. The resulting modified PCNCHFs were designated as PCNCHF0, PCNCHF1, PCNCHF2, PCNCHF3, PCNCHF4, and PCNCHF5, respectively.

2.3. Characterization

The developed PCNCHFs were characterized by different analytical methods. FTIR analysis was performed using a JASCO spectrophotometer and involved acquisition of spectra within the range of 4000 to 400 cm^{-1}. The XRD (Bruker AXN) spectra of PCNCHFs was examined in the wide angle 2θ value of 5°–85° using Copper-Kα radiation (λ = 1.5418 Å) at 30 kV and 40 mA. To measure morphological variations, all the PCNCHFs were coated with a thin Pt layer and then surveyed by FE-SEM at an acceleration voltage of 15–20 kV. In addition, quantitative elemental analysis was performed by EDX. To investigate their thermal properties, all PCNCHFs were subjected to DSC (NETZSCH DSC200F3) and TG (NETZSCH STA 409 PC, TGA-DTA) analysis. For DSC, the required amount of each sample (5 to 7 mg) was balanced and then studied between 25 °C and 350 °C at 5 °C/min heating increments. Similarly, TGA-DTA was performed until 600 °C from room temperature in the presence of a N_2 stream at 60 mL/min with increment in heating rate of 10 °C/min. The sepiolite mineral size was measured using DLS instrument. In addition, other methods were used to study the swelling, mechanical properties, drug loading, encapsulation efficiency, and biocompatibility of PCNCHFs, for which details are discussed in supplementary information.

3. Results and discussion

3.1. Fabrication of PCNCHFs

The present work is an extensive investigation on the hydrogels formation by blending of the biopolymers CMC and agar with other polymers. Simple moisture heat treatment of this polymer blend (CMC, agar, and PVP) reinforced with sepiolite mineral would result in a simultaneous physically cross-linked network formation via hydrogen-bond associated linear random coil configured macromolecules [41], leading to the formation of mechanically robust hydrogels through a one-pot and green method without using any chemical cross-linkers. The inclusion of PVP provides surface hydrophilicity and increases small-void formation. PVP is a hydrophilic, water-soluble polymer that has been shown to be cytocompatible and is capable of enhancing blood compatibility [42]. The graphical representation of this simple, economic, and rapid approach for composite hydrogel synthesis is illustrated in Fig. 1.

3.2. FTIR analysis

FTIR analysis yields useful evidence regarding the molecular structure, chemical bonding, and miscibility of polymers in multicomponent structures. Here, we used FTIR to examine the possible interactions of the as-prepared PCNCHF release systems. The FTIR spectra of sepiolite, pristine PCNCHFs, and their PCNCHFs@FU are provided in Fig. 2. In Fig. 2a, PCNCHF0 exhibits characteristic signals at 3480 cm^{-1} attributable to the stretching vibrations of hydroxyl groups. The peaks at 2890 and 1467 cm^{-1}, corresponds to C—H bending and C—N stretching vibrations are appeared at 1341, and 1243 cm^{-1}. Further, the carbonyl stretching vibrations in CMC and PVP are observed at 1660 cm^{-1}. The peaks at 1418 and 1359 cm^{-1} are due to strong and

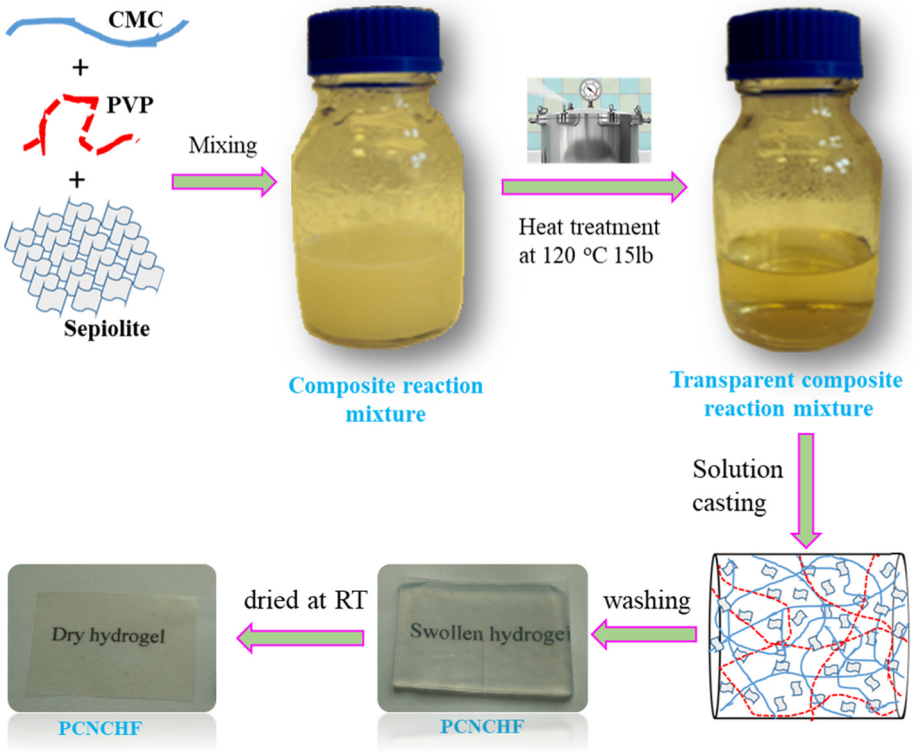

Fig. 1. Graphical illustration of the preparation of PCNCHFs.

medium C—N stretching vibrations. The peaks at 1151 to 1074 cm^{-1} are due to stretching vibrations of glycosidic ring (C–O–C) in CMC [43], and peaks at 959 and 839 cm^{-1} due to C—O and C—H bending vibrations, respectively. Similarly, pure sepiolite shows broad bands in the range 3900–3000, which is due to (free and intermolecular bonded) O—H stretching vibrations of silanols (Si–OH) and Mg–OH. The O—H bending vibrations of Si-OH, Mg-OH, are appeared at 1648 and 1461 cm^{-1}, respectively [44,45]. However, the intensity of these sepiolite peaks increased with increasing the sepiolite content in the polymer hydrogels. In PCNCHF5, the observed C—H stretching peak was reduced drastically at 2889 cm^{-1}; the absence of the C—H bond in pure sepiolite was evidenced by absence of C—H stretching vibrations in the PCNCHF5, which is the major indication of notable molecular dispersion of sepiolite. Furthermore, the peak at 1662.5 cm^{-1} was attributable to the bending vibration of zeolitic water, peaks at 1200 to 678 cm^{-1} were due to characteristic silicate, the peak at 1013.5 cm^{-1} was attributable to the presence of tetrahedral Si–O–Si bonds, peaks at 1185.7, 1063.4, and 937.3 cm^{-1} were attributable to Si—O bonds, and the peak at 689.3 cm^{-1} was attributable to Mg–OH bond vibrations [44]. These results evidenced the molecular dispersion of sepiolite inside the polymer hydrogel network. Furthermore, the thermodynamic parameters (E_a, ln$A$, ΔH, ΔS, and ΔG) for the two main thermal decomposition steps from 250 to 320 °C and 350–410 °C of the PCNCHFs were calculated using Broido's equation and their values were displayed in Tables 1 and 2, which is clearly explained in supplementary information.

As shown in Fig. 2b, the FT-IR spectra of PCNCHFs@FU showed characteristic peaks in the region of 3670–2750 cm^{-1} due to the N—H, O—H (Mg–OH, Si-OH), C—N, and C—H stretching vibrations of FU drug, sepiolite, CMC and PVP. The peaks at 2200 and 1420–1650 cm^{-1} correspond to the C═C and merged C═O & C═N stretching vibrations of FU drug, while the peaks at 1351 and 1242 cm^{-1} are due to the stretching vibration of the C—N (pyrimidine ring) and aromatic C—F stretching of FU drug. However, the intensity of the C–O–C and C—O stretching vibrations are reduced at 1149 and 1068 cm^{-1} due to the intercalation of FU in silicate layers of sepiolite. The peaks at 1252 and 500–800 cm^{-1} were corresponds to the C—N and aromatic ring stretching vibrations, respectively [10]. Finally, the pure FU drug peaks as mentioned in Fig. 2c. These results suggested that the intensity of the characteristic peaks of PCNCHFs are decreased due to intercalation of FU drug in the silicate layers of the sepiolite mineral, which caused decreased interaction between the FU drug and polymers. Herewith we conclude that molecular dispersion of FU drug, throughout the hydrogel network is uniform.

3.3. XRD analysis

XRD is a versatile and non-destructive technique that was performed to evaluate the influence of sepiolite reinforcement on the crystal structure of polymer hydrogels. The XRD patterns of pure sepiolite, FU, PCNCHFs, and FU-loaded PCNCHFs are shown in Fig. 2d. PCNCHF0 showed characteristic peaks at 12.7, 19.8, and 23.1 cm^{-1} ascribed to the semi-crystalline CMC and PVP polymers [41]. The semi-crystalline structure of both polymers was maintained by interactions between the monomer units via inter and intramolecular bonding [46]. Pure sepiolite shows a characteristic peak at 7.8° corresponding to the (110) crystalline plane. The peaks present in the range of 15° to 30° (23.5°, 28°, 31°) indicate the crystalline structure of silica in sepiolite. The peaks at 41° and 46° belong to sepiolite and those at 38° and 50° (JCPDS: 13-0595) are related to magnesite. In XRD analyses of PCNCHFs, a semi-crystalline region was prevalent at minimum concentrations (≤0.9 wt%) of sepiolite. Nevertheless, at a higher sepiolite concentration (≥1.5 wt%), low intense semi-crystalline peaks were noticed in PCNCHF5. The reduction in the semi-crystalline properties may be due to the interaction between the polar functionalities of both CMC and PVP polymers with the silicate layers in sepiolite. This retarded the ordering of the crystalline regions in the PCNCHF5 and resulted in a weak diffraction peak. As a result, PCNCHF5 showed low-intensity peaks at 9.06°, 12.79°, and 23.38°, respectively, and exhibited an amorphous nature. [47,48].

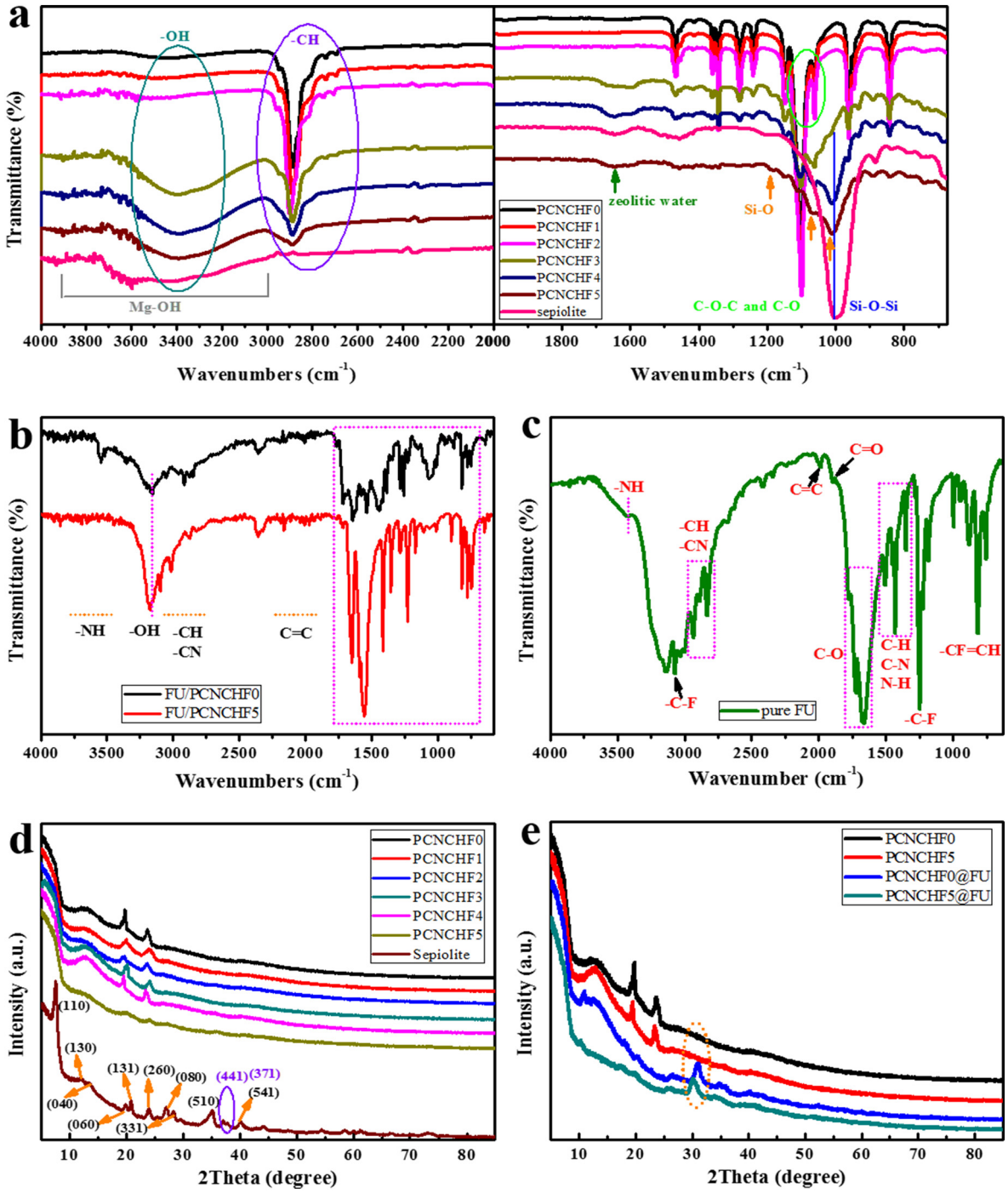

Fig. 2. FTIR analysis of (a) PCNCHFs, (b) PCNCHF@FU, and (c) pure FU; XRD spectra of PCNCHFs before (d) and after drug loading (e).

Table 1
The kinetic-thermodynamic parameters of PCNCHFs at the decomposition stage of 250–320 °C.

Title	E_a (kJ/mol) x 10^{-3}	ln*A*	ΔH (kJ/mol)	ΔS (kJ/K)	ΔG (kJ/mol)
Sepeolite	19.6620	−11.7589	−4.6390	−163.749	91.3706
PCNCHF0	478.861	−8.05612	−4.63224	−162.554	90.70371
PCNCHF1	402.306	−8.31591	−4.63338	−162.772	90.82547
PCNCHF2	370.557	−8.43276	−4.63385	−162.841	90.86382
PCNCHF3	348.074	−8.52062	−4.63419	−162.908	90.90122
PCNCHF4	364.305	−8.48939	−4.63394	−162.922	90.90892
PCNCHF5	242.965	−8.99547	−4.63575	−163.15	91.03634

For PCNCHFs@FU (Fig. 2e), the characteristic peaks related to sepiolite and both polymers were retained with weak diffraction peak intensities. In contrast, FU yielded an intense characteristic peak at 31.87°. The positions and intensities of the other peaks were shifted and evidently reduced, indicating a certain degree of interaction between FU and both polymers (CMC and PVP). The typical peaks of CMC and PVP polymers disappeared in both PCNCHF0@FU and PCNCHF5@FU. However, the sepiolite peaks appeared with less intensity because of the intercalation of FU in sepiolite layers, which caused an increase in the amorphous nature of the systems.

Table 2
The kinetic-thermodynamic parameters of PCNCHFs at the decomposition stage of 350–410 °C.

Title	E_a (kJ/mol) x 10^{-3}	ln*A*	ΔH (kJ/mol)	ΔS (kJ/K)	ΔG (kJ/mol)
Sepeolite	24.169	−11.7062	−5.42926	−162.908	106.384
PCNCHF0	698.414	−7.64433	−5.42067	−162.345	106.0159
PCNCHF1	822.164	−7.35961	−5.4191	−162.396	106.0497
PCNCHF2	783.18	−7.45104	−5.41959	−162.489	106.1099
PCNCHF3	687.706	−7.6789	−5.42081	−162.545	106.1469
PCNCHF4	598.082	−7.90457	−5.42195	−162.46	106.0913
PCNCHF5	505.285	−8.17296	−5.42313	−162.626	106.1995

3.4. SEM-EDX analysis

Morphological investigations of pristine (PCNCHF0) and sepiolite-reinforced polymer composite hydrogels (PCNCHF1 to PCNCHF5) were performed by SEM, as shown in Fig. 3. The SEM images showed that sepiolite reinforcement of the physical crosslinking network of polymers was properly connected together in the nanocomposites. The probable interactions between components can cause morphological changes in the nanocomposites. The SEM image of PCNCHF0 shows the physical morphology and surface characteristics of the network-like structure (Fig. 3a). The SEM findings for PCNCHF1 (Fig. 3b) showed that sepiolite incorporation inside the network enhances the interfacial interactions between the polar functions of CMC and PVP polymers and the silicate layers of sepiolite, and at a low concentration (0.3 wt%), the overlapping sepiolite layers exhibit a smooth surface morphology. However, at higher concentrations of sepiolite, the surface shows a plate-like structure, as shown in Fig. 3(b-f). At higher sepiolite (1.5 wt%) concentrations, PCNCHF5 displays a dense plate-like structure (Fig. 3f) along with the smooth surface caused by formation of the polymer-clay complex through interfacial interactions. These morphological changes confirm the reinforcement of sepiolite inside the physical hydrogel network.

EDX measurement was performed to evaluate the quantitative elemental data and their compositional characteristics. Therefore, EDX data of PCNCHF0 and PCNCHF5 were compared before and after sepiolite reinforcement. In Fig. 4a, the surface morphology of PCNCHF0 showed the presence of carbon, oxygen, and nitrogen, based on their atomic weights. These elements were derived from the polymers (i.e., CMC, PVP, and agar), with the presence of nitrogen confirming PVP. In contrast, PCNCHF5 (Fig. 4b) showed additional elements such as silicon and magnesium along with the aforementioned elements. Here, the carbon and nitrogen contents were reduced, whereas the oxygen, silicon, and magnesium contents were increased. These findings confirmed that the obtained PCNCHFs were successfully reinforced with the nano-sepiolite material.

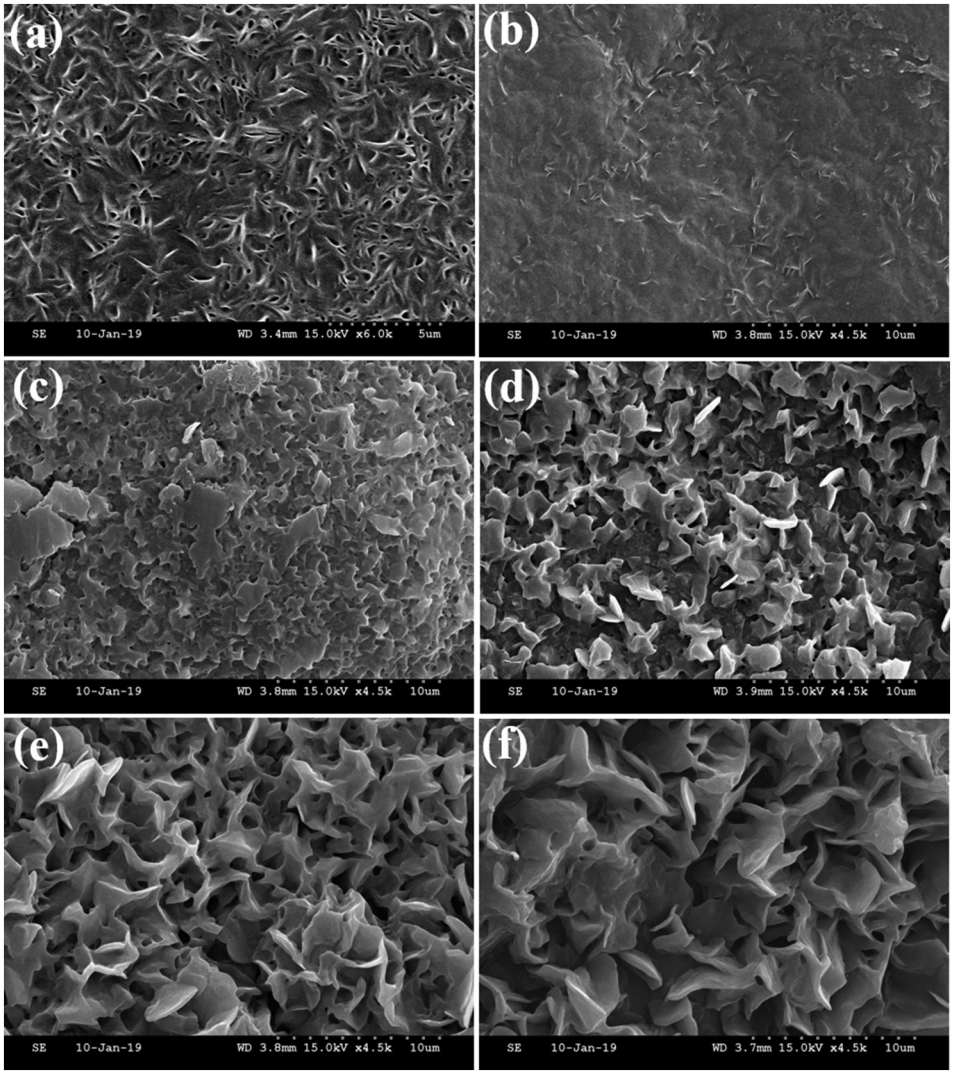

Fig. 3. Surface morphological features of all PCNCHFs measured in FE-SEM analysis.

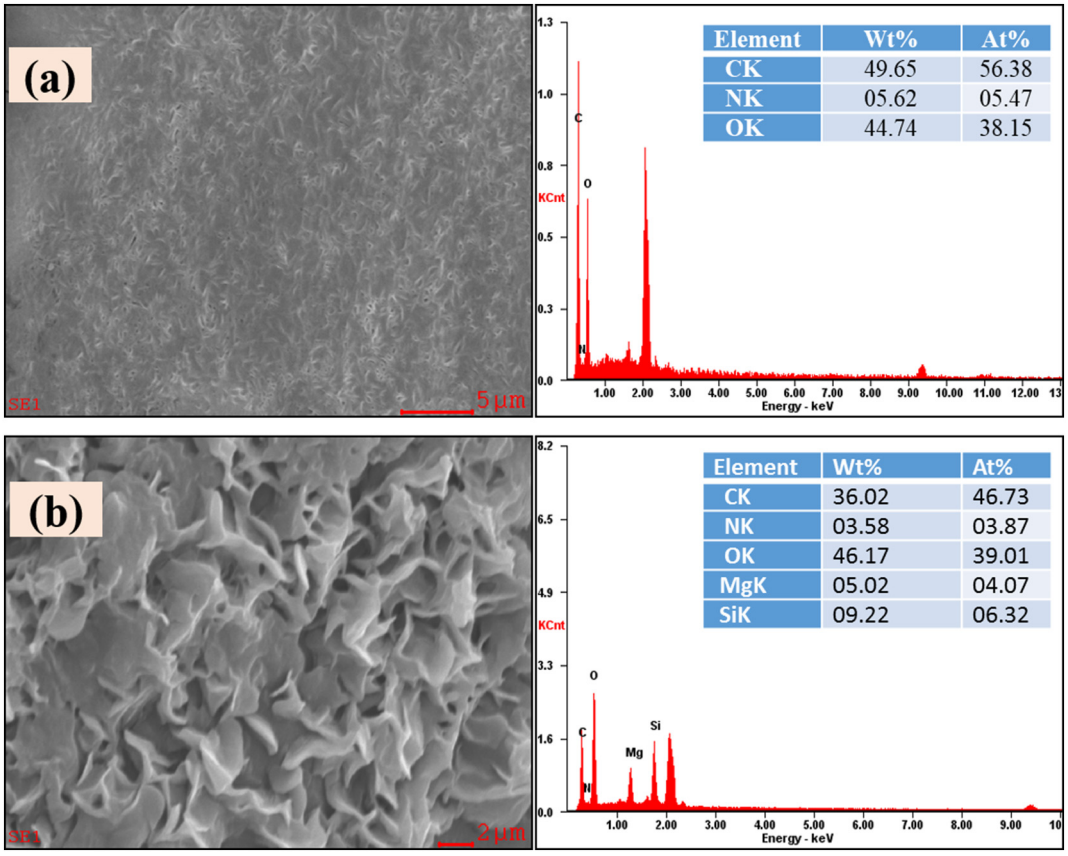

Fig. 4. SEM-EDX analysis of (a) PCNCHF0 and (b) PCNCHF5.

3.5. Thermal analysis

3.5.1. DSC analysis

DSC investigations play a vital role in characterizing a material's thermal properties, which are associated with their transition states, structure, and hydrophilicity, and can further confirm the interactions between polymers and sepiolite. The thermal behavior of the PCNCHFs and the FU-loaded PCNCHFs was examined by DSC thermograms in the spectral range of 30–350 °C, and all curves showed endothermic and exothermic peaks, as shown in Fig. 5(a-b). In Fig. 5a, the primary transition of DSC detected at 50–125 °C was attributed to the glass-transition temperature (Tg) for primary relaxation of polymer chains because of micro-Brownian motion of the polymer backbones and silicate layers. Moreover, this endotherm represents the elimination of residual moisture in the PCNCHFs. In addition, the sharp T_g of PCNCHFs specifies the synergy among polymers and sepiolite. As sepiolite content (0.3% to 1.5%) increases in polymer matrix, it will eventually increases the T_g and T_m values from PCNCHF1 to PCNCHF5. These characteristics are highly relevant when the hybrid material is developed as a carrier system for bioactive materials. Consequently, the hybrid materials show effective changes in various properties in comparison with pristine polymers and PCNCHF0, such as swelling, thermal, mechanical strength, strain modulus, and fracture resistance properties. The broad exothermic peak of PCNCHFs at 225–260 °C was attributed to the melting temperature (T_m), due to the presence of semi-crystallinity in polymers. The nature of the T_m peak indicates the drop-in crystallinity of PCNCHF0 (semi-crystalline) and the upsurge of the amorphous segment from PCNCHF1 to PCNCHF5, in agreement with the findings of XRD.

As shown in Fig. 5b, the DSC thermograms provide information regarding the physico-chemical properties of drug entrapment by PCNCHFs. During the first transition, the PCNCHF0@FU and PCNCHF5@FU showed a broad endothermic peak at around 60 °C–120 °C due to evaporation of residual water molecules. According to the literature [8,49], FU alone exhibits a sharp peak at 284 °C corresponding to its melting and polymorphism. In addition, the peak depth at T_m specifies the reduced crystallinity in PCNCHFs@FU and the increased amorphous fraction in PCNCHF0@FU and PCNCHF5@FU, in agreement with the FTIR results. However, this FU peak alone was not observed after loading into the PCNCHFs. These findings confirm that the FU was molecularly dispersed into the PCNCHFs network, which is in the amorphous state, and that PCNCHF@FU remained unaffected during encapsulation.

3.5.2. TGA analysis

The influence of sepiolite reinforcement on the polymer composite hydrogels was investigated to verify the thermal stability and the extent of degradation by integral TGA and DTG curves, as shown in Fig. 5(c-d). In Fig. 5c, pure sepiolite shows three distinct degradation steps. In the first step, sepiolite undergoes weight loss of 9.2% due to elimination of the absorbed water molecules on the zeolitic surface from 25 °C to 130 °C. The second degradation was observed from 130 °C to 305 °C and was attributed to the loss of weakly bound coordinated water, with a 3% loss of weight. The third degradation step was detected from 305 °C to 525 °C, and was ascribed to the dehydration of firmly bonded coordinated water, similar to the second major degradation step. Lastly, 1.6% weight loss was observed after 650 °C which shows dihydroxylation followed by structural obliteration.

The PCNCHFs show three distinguishable degradation steps in the TGA diagram, which appear more clearly in the DTG diagram. The degradation steps from PCNCHF0 to PCNCHF5 as follows: 1) the initial degradation between 35 °C and 180 °C with 9.5%, 9.4%, 9.12%, 9.1%, 8.6%, and 7.8% weight loss respectively, which indicates the elimination of physically adsorbed/ hydrogen bond linked water molecules; 2) the second degradation step between 250 °C and 320 °C with 24.3%, 22.7%, 21.4%, 20.7%, 21.0%, and 16.1% weight loss, respectively; and 3) the final

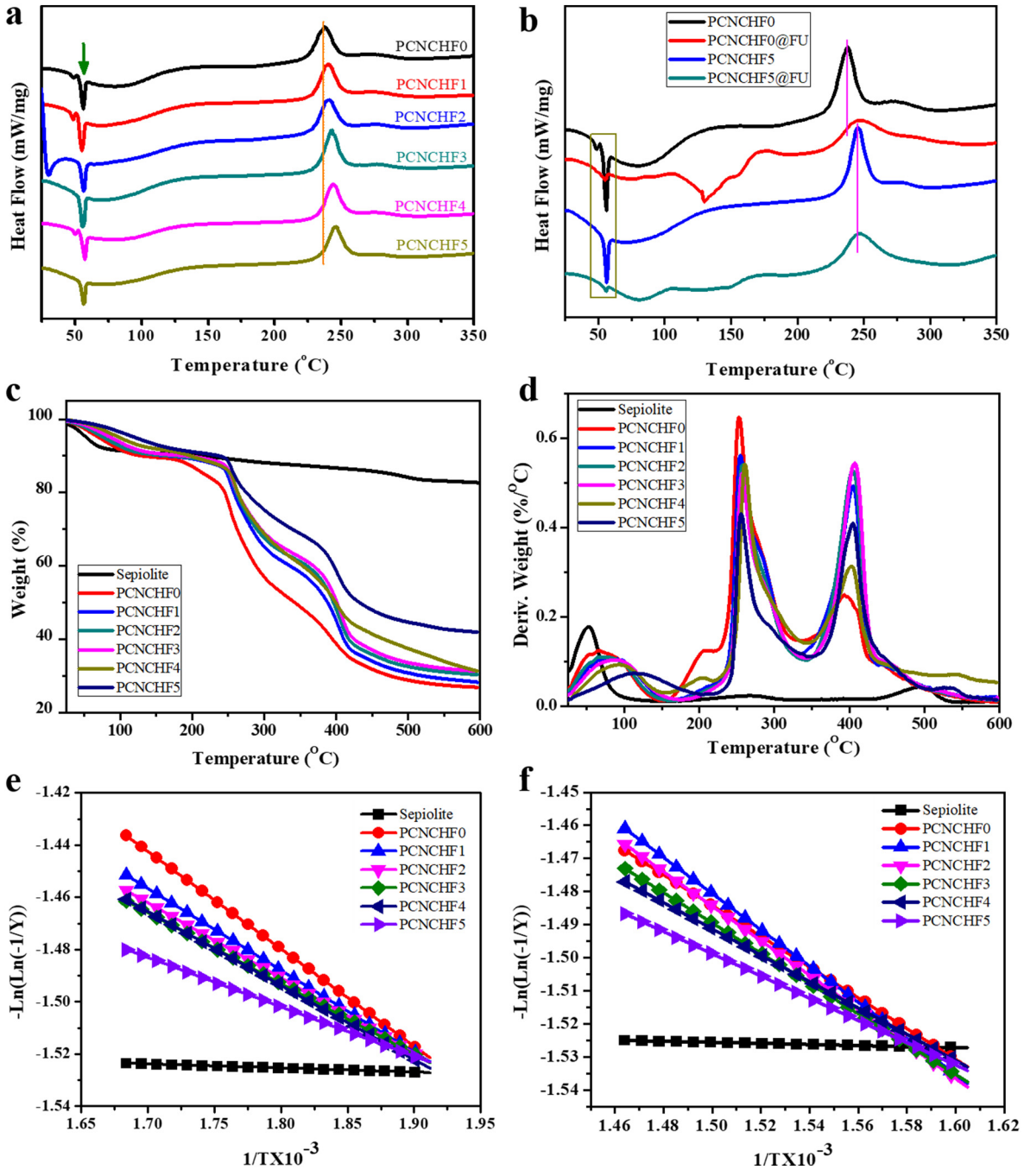

Fig. 5. (a-b) DSC analysis of PCNCHFs and PCNCHF@FU; (c-d) TGA analysis of PCNCHFs, and plots of −Ln(ln(−1/Y)) vs 1/T for decomposition steps in the range of (e) 250–320 °C and (f) 350–410 °C, respectively).

degradation from 350 °C to 410 °C with 12.3%, 17.8%, 18.0%, 16.9%, 13.6%, and 14.0% weight loss, respectively. However, the initial weight loss was attributable to both the elimination of substantially adsorbed/hydrogen bonded water and the increase in the glass transition temperature from PCNCHF0 to PCNCHF5. The second weight loss corresponded to the removal of zeolitic water and weakly bound coordinated water, which indicated the increase in the melting temperature after sepiolite incorporation. The final weight loss occurred due to dehydroxylation and structural destruction of PCNCHFs. All degradation steps were clearly observed by the DTG diagram (Fig. 5d). On the basis of the results, we concluded that the sepiolite content increases and then decreases the weight loss and increases the percentage of weight remaining (Fig. S2). The increased uniform molecular dispersion and interfacial interactions between polar polymer groups and silicate layers of sepiolite potentially enhanced the thermal stability of PCNCHFs. Furthermore, the thermodynamic parameters (E_a, ln$A$, ΔH, ΔS, and ΔG) for the two main thermal decomposition steps from 250 to 320 °C and 350–410 °C of the PCNCHFs were calculated using Broido's equation, which is clearly explained in supplementary information.

3.6. Swelling study

The water holding capability of PCNCHFs was calculated by measuring the percentage swelling ratio (%SR). The %SR calculations were performed by determining the dry weight (50 mg) of all PCNCHFs dipped in water for shorter and longer duration (30 min and 38 h) and displayed in Fig. 6a. From the plot, the %SR values of PCNCHFs are clearly contingent on the immersion time and the incorporated sepiolite

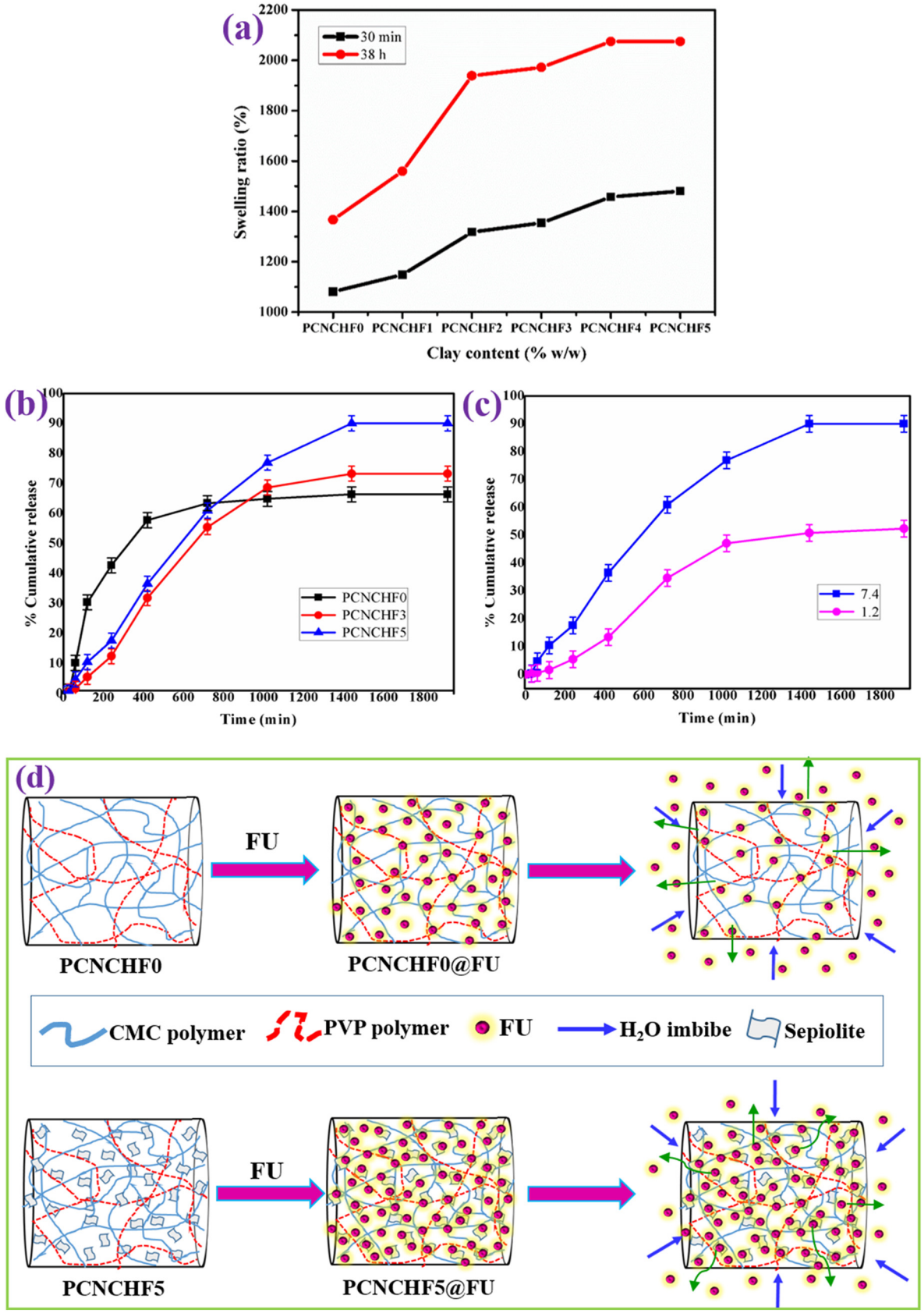

Fig. 6. Analyses of PCNCHF (a) swelling, (b-c) in vitro FU release at pH = 7.4 and 1.2 in PBS at RT, and (d) release mechanism.

content. The %SR for PCNCHF0 increased >1.2 times with the immersion time (from 30 min to 38 h), while it increased approximately 1.6 times with an increase in the clay content (from 0 to 1.5%) for both immersion times. The hydrophilicity of sepiolite clay is a key parameter responsible for the upsurge in %SR values with an increase in sepiolite content. The PCNCHF5 samples showed high water-holding capability with

significant mechanical strength and moderate flexibility. In this regard, the enhanced water resistance of biopolymer films with reinforcement of nanoclay has been observed for various composites like CMC/starch/clay, chitosan/clay, and agar/clay nanocomposite films [33,36,50]. This is due to the H-bond interaction between the –OH functional groups and the biopolymer chains. The high surface area of sepiolite improves the compact packing of biopolymer matrix with sepiolite, decreasing its sensitivity to water [51]. The unique characteristics of these superporous PCNCHFs open a new window into controlled drug/bioactive compound delivery application.

3.7. Cumulative release of FU

The PCNCHFs showed a pH-responsive drug-release behavior due to presence of acid functional groups. The effect of different functional polymer groups on FU encapsulation and their release kinetics were determined. The EE of PCNCHF3 (37%) and PCNCHF5 (45%) were higher than that of PCNCHF0 (25%) due to the enhanced porosity as a result of the interaction between the functional polymer and sepiolite and the consequently increased penetration of drug molecules. Moreover, the uniformity of the topological structure of nano-sepiolite and its surface charges permitted higher drug loading into the composite hydrogel. Thus, the drug-loaded polymer–clay composite hydrogels (PCNCHF3@FU and PCNCHF5@FU) showed higher FU release at pH 7.4 and 1.2 than the polymer hydrogel (PCNCHFF0@FU, as depicted in Fig. 6b & 6c). The increase in sepiolite concentration from PCNCHF1 to PCNCHF5 increased %FU release because of the network porosity increment as a result of sufficient surface interactions between the polymers and the clay structure. In contrast, the reduced FU release with a further increase in sepiolite concentration can be attributed to the non-homogeneous structure (data not shown). However, the PCNCHF5@FU showed higher FU release at pH 7.4 compared to the FU release from PCNCHF0@FU at pH 1.2 (Fig. 6c). The reason for this is that at high pH, the polymer acid groups were ionized (–COOH → –COO$^-$) to

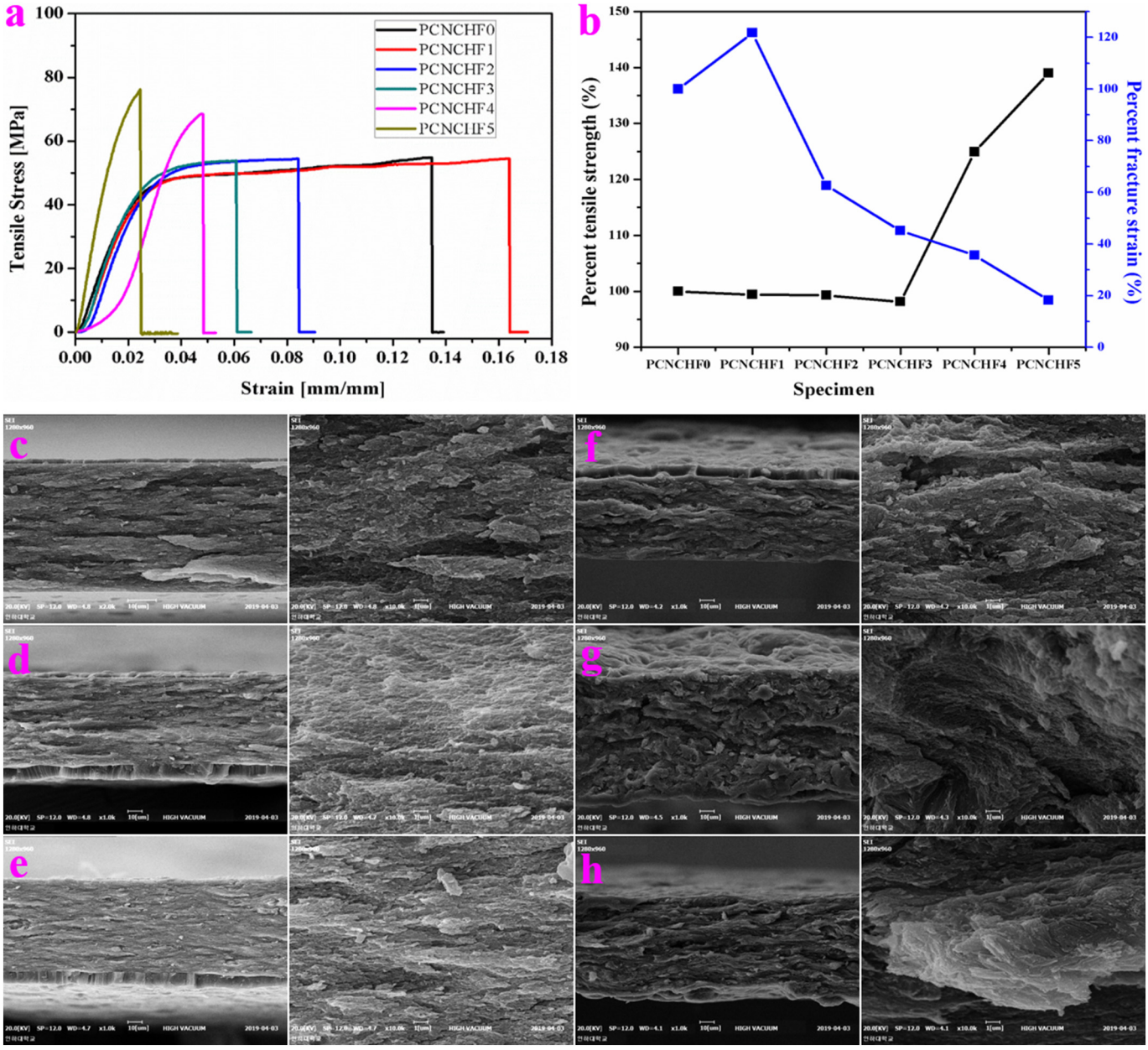

Fig. 7. Mechanical properties of PCNCHFs. (a) Stress-strain curves, (b) percentage changes in the tensile strength vs. fracture stress, and (c-h) SEM morphology of the tensile fracture surface. The SEM images are shown with low and high magnifications, as indicated.

create osmotic pressure on the composite network; moreover, this $-COO^-$ increased the electrostatic repulsive forces, leading to lower hydrogen bonding, and the resultant swelling changes led to further FU release in a sustained manner [5,8,49]. Furthermore, the interaction of sepiolite with CMC macromolecules instigated the inhibition of FU leakage during the formation of the composite hydrogels. This could also be one of the reasons for the decrease in FU vanishment from the PCNCHFs [52]. In contrast, at pH 1.2, protonation of the acid groups reduced the electrostatic forces among the $-COO^-$ groups, which reduced the hydrogen-bonding association and eventually reduced FU release because of absorption shrinking. The release kinetics of PCNCHF5@FU were compared with those of PCNCHF3@FU and PCNCHF0, which confirmed the prolonged and sustained release of FU from the network. In this process, the nano-clay plays a crucial part in the course of FU release. The FU release time of PCNCHF5@FU was extended for 32 h owing to the longer route for FU migration from PCNCHF5 to the PBS medium due to the greater porosity created by nano-sepiolite, in comparison with PCNCHF0. The FU release mechanism of PCNCHFs is depicted in Fig. 6d, as follows: the nano-sepiolite particles in the composite structure provided a longer route for FU migration into the PBS medium compared to PCNCHF0 [52]. This prolonged the release time of FU in a well-controlled manner.

For the evaluation of FU release mechanism from all PCNCHFs, the release kinetic parameters played an important role and were determined by plotting the graph between Mt./M∞ (cumulative release) and t (time). Herein, the values were applied in $Mt./M\infty = Kt^n$, then the "n" values were between the 0.49 and 0.60, which suggests that the PCNCHFs@FU followed an anomalous FU transport model with two explicitly independent mechanisms: diffusion-controlled (non-Fickian) and case II transport (swelling controlled) [5,10]. Both extended drug release time and sustained release performance offer advantages in cancer treatment proficiency since the stable and persistent drug release from the carrier can efficiently kill cancer cells and prevent their growth in long-term usage.

3.8. Mechanical properties

Reinforcement of the polymer hydrogels with different concentrations of sepiolite, greatly influenced their mechanical properties, which were studied by tensile measurements, and the findings are depicted in Fig. 7a. With the increase in sepiolite content from PCNCHF0 (0% sepiolite) to PCNCHF5 (1.5% sepiolite), the tensile strength (TS) also increased from 52.04 ± 0.68 MPa to 78.02 ± 0.76 MPa, although further reinforcement of clay decreased the mechanical properties. A similar pattern was reported earlier for gelatin-egg white/clay biopolymer nanocomposite [53], CMC/starch/clay [33], chitosan/clay [36], and agar/clay [50]. These findings can be attributed to the conformation developed by the nano-fibrous structures of sepiolite with a surface area of 320 m^2/g [28,38]. The ionic interactions and Van der Waals forces between polymer chains and silanol groups (Si–OH) yielded well-assembled polymer–clay nanocomposite structures [33]. In contrast, PCNCHF0 showed increased toughness, resulting in a higher elastic modulus and yield stress. The reinforcement of sepiolite has a stronger impact on the elastic modulus. In this system, the physical crosslinking interactions among CMC and PVP are accompanied by hydrogen bonds created between CMC and PVP and CMC and sepiolite, which generate a higher number of entanglements and build up a stronger network. However, the reinforcement of sepiolite beyond 1.5% did not affect the properties of nanocomposites; this may be due to uneven distribution of sepiolite, which created stacked structures at higher concentrations. As shown in the Fig. 7(b), the tensile strength of the PCNCHF5 (78.02 ± 0.76 MPa) was ~109% higher than that for the PCNCHF0. Therefore, the increment of sepiolite inside the polymer matrix can greatly influence the mechanical properties of the PCNCHF0, which eventually optimizes the physical cross-linking inside the network structure of nanocomposites. Comparatively, the TS values of PCNCHF1 to PCNCHF5 are higher than those of industrial trade polymer films such as high-density polyethylene, polypropylene, and polystyrene, which show TS values of 22–31, 31–38, and 45–83 MPa, respectively [54].

The tensile fracture surface of PCNCHFs was observed by SEM analysis. Fig. 7(c-h) shows the overall morphology of the fractured surfaces (in different magnifications). The pristine PCNCHF0 displayed quite soft textured surface (Fig. 7c), whereas the intercalated nanocomposites from PCNCHF1 to PCNCHF3 showed a somewhat uneven cracked distribution pattern (Fig. 7d-f) and at high magnifications, these patterns were predominant (Fig. 7d-f). As the sepiolite reinforcement increased from PCNCHF4 to PCNCHF5, the resultant PCNCHFs did not show any presiding layered intricated structures in the low-magnification image. However, high-resolution images clearly depicted the assemblage of nanosized sepiolite clay particles distributed evenly throughout the polymer matrix (Fig. 7g-f).

3.9. In vitro cytocompatibility of the polymer hydrogels

Despite showing profound mechanical properties, chemical stability, ease of processing, and non-toxic nature, cytocompatibility remains an essential parameter for any material before it can be used in biomedical applications. Therefore, we assessed CCDK cell attachment to all the PCNCHFs to demonstrate their cytotoxicity and cytocompatibility behavior since fibroblasts plays a prime role in the formation of granulation tissue and tissue regeneration. To evaluate the cytotoxicity and cell viability, the pristine and sepiolite-incorporated polymer hydrogels against CCDK cells were assessed using PrestoBlue, which allows simple and rapid live measurement for toxicity and viability. Fig. 8 demonstrates the percentage cell viability of CCDK exposed to PCNCHF0, PCNCHF1, PCNCHF3, PCNCHF4, and PCNCHF5 for a 72-h incubation period. The obtained results confirmed that the all PCNCHFs showed >95% cell viability, which is comparable to the control groups and other polymer-clay composites [55]. Therefore, the developed PCNCHFs are non-toxic to normal cells, indicating their excellent biocompatibility.

Moreover, biocompatibility was further assessed by measurements of live/dead cells and their images were obtained by fluorescence microscopy. As shown in Fig. 9, the live cells and dead cells were measured with green and red fluorescence, respectively. The fibroblasts seeded to PCNCHFs were found to remain feasible after 72-h culture, which exhibited strong green fluorescent cells. As the sepiolite reinforcement increased in the hydrogels, the number of elliptical/round-shaped fibroblasts increased gradually. At higher sepiolite concentrations, the

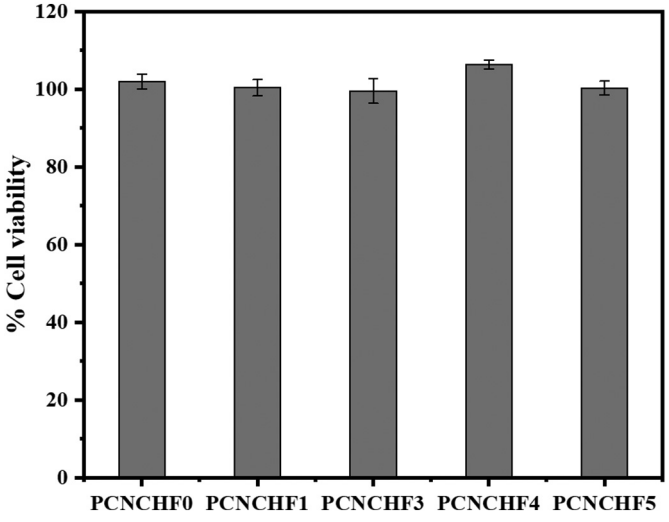

Fig. 8. Prestoblue-based cell viability assay against fibroblasts (CCDK) treated with different hydrogel samples for a 72-h incubation period.

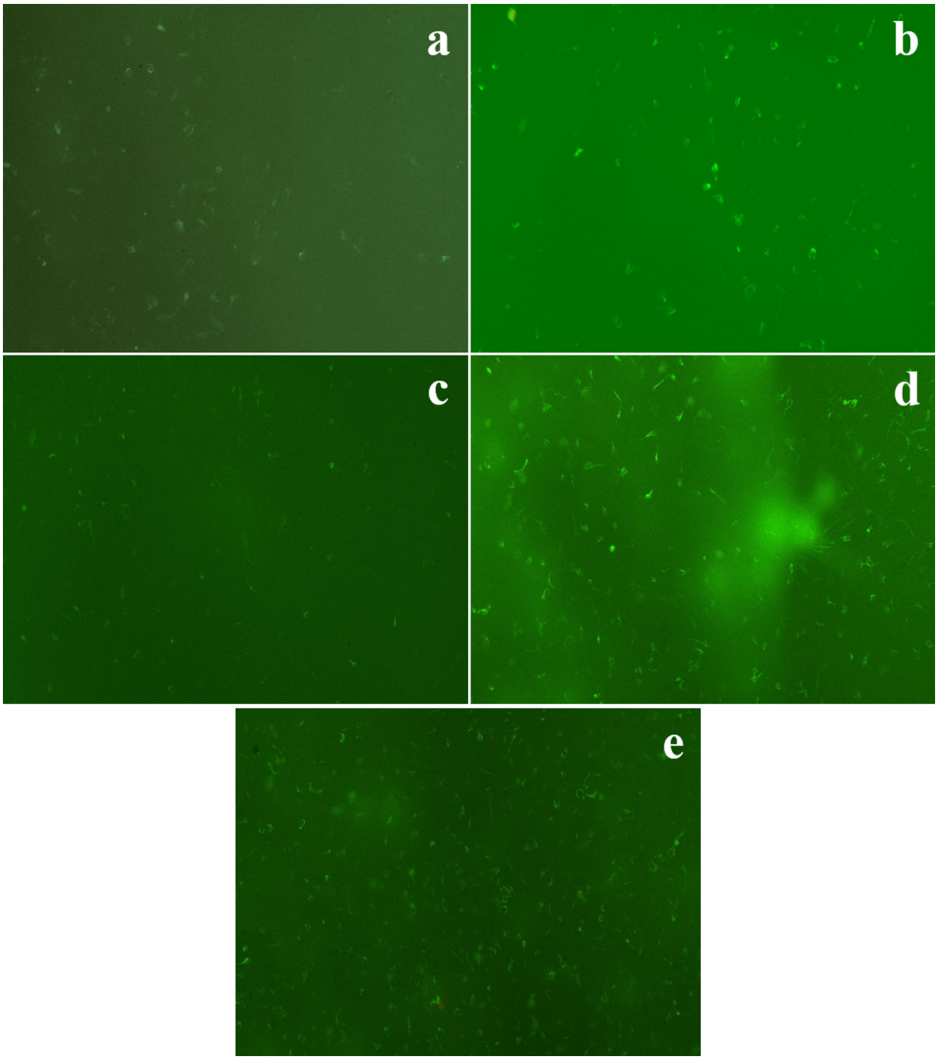

Fig. 9. Live/dead assay fluorescence images of human skin fibroblasts (CCDK) cells (a-e) treated with hydrogel samples (PCNCHF0 to PCNCHF5) for a 72-h incubation period. The images were captured with a 200-μm scale bar. The live and dead cells were indicated by green and red colors, respectively.

elliptical/round-shaped fibroblasts were consistently dispersed in the network structure, which indicated the excellent biocompatibility of PCNCHFs. These results suggested that the PCNCHFs had good cytocompatibility along with a non-toxic nature. The porous network structure of PCNCHFs, which permitted oxygen and nutrients to permeate, provided an appropriate ambiance for fibroblasts. Therefore, the developed PCNCHFs could be used in different fields such as drug delivery, tissue engineering, wound dressing, and food packaging applications to not only provide physical support but also improve the survivability of normal cells via their interactions with the cell membrane receptors.

4. Conclusion

In this study, CMC-based hydrogels reinforced with sepiolite (PCNCHFs) were successfully developed by moist heat treatment followed by solution casting. The FTIR spectra of PCNCHFs displayed some distinct changes in the spectral range with a difference in their vibrational band intensities representing an interfacial interaction among the polar groups (carboxylic, hydroxyl, and imine) of the polymers and silanol groups (Si-OH) on sepiolite. The XRD results showed that reinforcement of sepiolite on the polymer hydrogels resulted in reduced crystallinity. Subsequently, the surface morphology of PCNCHFs was modified with layer, plate, and cluster-type formations, respectively. The peak depth at glass transition and melting point from DSC analysis also showed a decrease in the degree of crystallinity of PCNCHFs and the increase of the amorphous nature, which was consistent with the XRD results. The TG thermograms of PCNCHFs moved toward higher temperature after sepiolite reinforcement, confirming the good dispersion and strong interfacial interactions between silanol (Si–OH) groups of sepiolite and the carbonyl, carboxylic acid, imine, and hydroxyl groups of polymers, which improved the thermal stability of PCNCHFs. The TS of PCNCHF5 (78.8 MPa) was higher than that of the pristine PCNCHF0 (53.2 MPa). The PCNCHFs exhibited biocompatibility and showed higher swelling capacity with stable and sustained FU release in time, which is more favorable for different drug release applications. On the basis above investigation results, PCNCHFs may offer a simple, economic, and unique approach for the fabrication of novel systems that will be useful in different fields, including drug delivery, wound dressing, tissue engineering, and food packaging.

CRediT authorship contribution statement

Ramasubba Reddy Palem: Conceptualization; Data curation; Formal analysis; Writing – original draft. **K. Madhusudana Rao:**

Biocompatibility analysis. **Ganesh Shimoga:** Formal analysis; kinetic-thermodynamic parameter calculations; Review & editing. **Rijuta G. Saratale:** Formal analysis; Review & editing. **Surendra K. Shinde:** Formal analysis; Review & editing. **Gajanan S. Ghodake:** Formal analysis; Review & editing. **Soo-Hong Lee:** Supervision; Formal analysis; & funding.

Declaration of competing interest

The authors declare no conflict of interest.

Acknowledgments

This work was supported by the National Research Foundation of Korea (NRF) grant funded by the Korea government (MSIT) (NRF-2019R1A2B5B03069690 and NRF-2019M3A9H1032376).

Appendix A. Supplementary data

Supplementary data to this article can be found online at https://doi.org/10.1016/j.ijbiomac.2021.02.195.

References

[1] Antony V. Samrot, Tan Chuan Sean, Teeshalini Kudaiyappan, Ummu Bisyarah, Anita Mirarmandi, Etel Faradjeva, Amira Abubakar, Hawwa Hashma Ali, J. Lavanya Agnes Angalene, S. Suresh Kumar, Production, characterization and application of nanocarriers made of polysaccharides, proteins, bio-polyesters and other biopolymers: a review, Int. J. Biol. Macromol. 165 (2020) 3088–3105, https://doi.org/10.1016/j.ijbiomac.2020.10.104.

[2] M.M. Orta, J. Martín, J.L. Santos, I. Aparicio, S. Medina-Carrasco, E. Alonso, Biopolymer-clay nanocomposites as novel and ecofriendly adsorbents for environmental remediation, Appl. Clay Sci. 198 (2020), 105838, https://doi.org/10.1016/j.clay.2020.105838.

[3] M.L. Verma, B.S. Dhanya, V. Rani Sukriti, M. Thakur, J. Jeslin, R. Kushwaha, Carbohydrate and protein based biopolymeric nanoparticles: current status and biotechnological applications, Int. J. Biol. Macromol. 154 (2020) 390–412, https://doi.org/10.1016/j.ijbiomac.2020.03.105.

[4] S.J. Hossieni-Aghdam, B. Foroughi-Nia, Z. Zare-Akbari, S. Mojarad-Jabali, H. motasadizadeh, H. Farhadnejad, Facile fabrication and characterization of a novel oral pH-sensitive drug delivery system based on CMC hydrogel and HNT-AT nanohybrid, Int. J. Biol. Macromol. 107 (2018) 2436–2449, https://doi.org/10.1016/j.ijbiomac.2017.10.128.

[5] R.R. Palem, G. Shimoga, T.J. Kang, S.H. Lee, Fabrication of multifunctional Guar gum-silver nanocomposite hydrogels for biomedical and environmental applications, Int. J. Biol. Macromol. 159 (2020) 474–486, https://doi.org/10.1016/j.ijbiomac.2020.05.041.

[6] T. Kopač, A. Ručigaj, M. Krajnc, The mutual effect of the crosslinker and biopolymer concentration on the desired hydrogel properties, Int. J. Biol. Macromol. 159 (2020) 557–569, https://doi.org/10.1016/j.ijbiomac.2020.05.088.

[7] S. Sharma, S. Tiwari, A review on biomacromolecular hydrogel classification and its applications, Int. J. Biol. Macromol. 162 (2020) 737–747, https://doi.org/10.1016/j.ijbiomac.2020.06.110.

[8] P.R.S. Reddy, K.M. Rao, K.S.V.K. Rao, Y. Shchipunov, C.S. Ha, Synthesis of alginate based silver nanocomposite hydrogels for biomedical applications, Macromol. Res. 22 (8) (2014) 832–842, https://doi.org/10.1007/s13233-014-2117-7.

[9] P.R.S. Reddy, S. Eswaramma, K.S.V. Krishna rao, Y.I. Lee, Dual responsive pectin hydrogels and their silver nanocomposites: swelling studies, controlled drug delivery and antimicrobial applications, Bull. Kor. Chem. Soc. 35 (8) (2014) 2391–2399.

[10] K. Sangsuriyonk, N. Paradee, A. Sirivat, Electrically controlled release of anticancer drug 5-fluorouracil from carboxymethyl cellulose hydrogels, Int. J. Biol. Macromol. 165 (2020) 865–873, https://doi.org/10.1016/j.ijbiomac.2020.09.228.

[11] S. Javanbakht, A. Shaabani, Carboxymethyl cellulose-based oral delivery systems, Int. J. Biol. Macromol. 133 (2019) 21–29, https://doi.org/10.1016/j.ijbiomac.2019.04.079.

[12] T. Agarwal, S.N.G.H. Narayanaa, K. Pal, K. Pramanik, S. Giri, I. Banerjee, Calcium alginate-carboxymethyl cellulose beads for colon-targeted drug delivery, Int. J. Biol. Macromol. 75 (2015) 409–417, https://doi.org/10.1016/j.ijbiomac.2014.12.052.

[13] S. Javanbakht, A. Hemmati, H. Namazi, A. Heydari, Carboxymethylcellulose-coated 5-fluorouracil@MOF-5 nano-hybrid as a bio-nanocomposite carrier for the anticancer oral delivery, Int. J. Biol. Macromol. 155 (2020) 876–882, https://doi.org/10.1016/j.ijbiomac.2019.12.007.

[14] M. Culebras, A. Barrett, M. Pishnamazi, G.M. Walker, M.N. Collins, Wood-derived hydrogels as a platform for drug-release systems, ACS Sustain. Chem. Eng. 9 (2021) 2515–2522, https://doi.org/10.1021/acssuschemeng.0c08022.

[15] R. Rakhshaei, H. Namazi, A potential bioactive wound dressing based on carboxymethyl cellulose/ZnO impregnated MCM-41 nanocomposite hydrogel, Mater. Sci. Eng. C 73 (2017) 456–464, https://doi.org/10.1016/j.msec.2016.12.097.

[16] U. Maver, K. Xhanari, M. Žižek, L. Gradišnik, K. Repnik, U. Potočnik, M. Finšgar, Carboxymethyl cellulose/diclofenac bioactive coatings on AISI 316LVM for controlled drug delivery, and improved osteogenic potential, Carbohydr. Polym. 230 (2020), 115612, https://doi.org/10.1016/j.carbpol.2019.115612.

[17] V. Bampidis, G. Azimonti, Md.L. Bastos, H. Christensen, B. Dusemund, M.K. Durjava, M. Kouba, M. López-Alonso, S.L. Puente, F. Marcon, B. Mayo, A. Pechová, M. Petkova, F. Ramos, Y. Sanz, R.E. Villa, R. Woutersen, G. Bories, J. Gropp, C. Nebbia, M.L. Innocenti, G. Aquilina, Safety and efficacy of sodium carboxymethyl cellulose for all animal species, Scientific Opinion 18 (7) (2020), e06211, https://doi.org/10.2903/j.efsa.2020.6211.

[18] C.B. Hollabaugh, L.H. Burt, A.P. Walsh, Carboxymethylcellulose. Uses and applications, Ind. Eng. Chem. 37 (1945) 943–947, https://doi.org/10.1021/ie50430a015.

[19] S.B. Sengel, M. Sahiner, N. Aktas, N. Sahine, Halloysite-carboxymethyl cellulose cryogel composite from natural sources, Appl. Clay Sci. 140 (2017) 66–74https://doi.org/10.1016/j.clay.2017.01.031.

[20] A. Baran, E. Sulukan, M. Türkoğlu, A. Ghosigharehagaji, S. Yildirim, M. Kankaynar, I. Bolat, M. Kaya, A. Topal, S.B. Ceyhun, Is sodium carboxymethyl cellulose (CMC) really completely innocent? It may be triggering obesity, Int. J. Biol. Macromol. 163 (2020) 2465–2473, https://doi.org/10.1016/j.ijbiomac.2020.09.169.

[21] R. Suriyatem, N. Noikang, T. Kankam, K. Jantanasakulwong, N. Leksawasdi, Y. Phimolsiripol, C. Insomphun, P. Seesuriyachan, T. Chaiyaso, P. Jantrawut, S.R. Sommano, T.M.P. Ngo, P. Rachtanapun, Physical properties of carboxymethyl cellulose from palm bunch and bagasse agricultural wastes: effect of delignification with hydrogen peroxide, Polymers 12 (2020) 1505, https://doi.org/10.3390/polym12071505.

[22] S.J. Hossieni-Aghdam, B. Foroughi-Nia, Z. Zare-Akbari, S. Mojarad-Jabali, H. motasadizadeh, H. Farhadnejad, Facile fabrication and characterization of a novel oral pH-sensitive drug delivery system based on CMC hydrogel and HNT-AT nanohybrid, Int. J. Biol. Macromol. 107 (2018) 2436–2449, https://doi.org/10.1016/j.ijbiomac.2017.10.128.

[23] B. Gaihre, A.C. Jayasuriya, Fabrication and characterization of carboxymethyl cellulose novel microparticles for bone tissue engineering, Mater. Sci. Eng. C 69 (2016) 733–743, https://doi.org/10.1016/j.msec.2016.07.060.

[24] V. Kanikireddy, K. Varaprasad, T. Jayaramudu, C. Karthikeyan, R. Sadiku, Carboxymethyl cellulose-based materials for infection control and wound healing: a review, Int. J. Biol. Macromol. 164 (2020) 963–975, https://doi.org/10.1016/j.ijbiomac.2020.07.160.

[25] J.S. Yaradoddi, N.R. Banapurmath, S.V. Ganachari, M.E.M. Soudagar, N.M. Mubarak, S. Hallad, S. Hugar, H. Fayaz, Biodegradable carboxymethyl cellulose based material for sustainable packaging application, Sci. Report. 10 (2020) 21960, https://doi.org/10.1038/s41598-020-78912-z.

[26] R.G. Garduque, B.J. Gococo, C.A. Yu, P.J. Nalzaro, T. Tumolva, Synthesis and characterization of sodium carboxymethyl cellulose/sodium alginate/hydroxypropyl cellulose hydrogel for agricultural water storage and controlled nutrient release, Solid State Phenom. 304 (2020) 51–57, https://doi.org/10.4028/www.scientific.net/ssp.304.51.

[27] S. Saber-Samandari, S. Saber-Samandari, S. Heydaripour, M. Abdouss, Novel carboxymethyl cellulose based nanocomposite membrane: synthesis, characterization and application in water treatment, J. Environ. Manag. 166 (2016) 457–465, https://doi.org/10.1016/j.jenvman.2015.10.045.

[28] A. Alvarez, J. Santarén, A. Esteban-Cubillo, P. Aparicio, Current industrial applications of palygorskite and sepiolite. In: Galán, E., Singer, A.A. (Eds.), Advances in the Crystal Chemistry of Sepiolite and Palygorskite. Developments in Palygorskite–Sepiolite Research. Developments in Clay Science (Dev. Clay Sci.) vol. 3 (2011) 281–298. doi: https://doi.org/10.1016/B978-0-444-53607-5.00012-8.

[29] W. Wang, A. Wang, Nanoscale clay minerals for functional Ecomaterials: Fabrication, applications, and future trends, in: L. Martínez, O. Kharissova, B. Kharisov (Eds.), Handbook of Ecomaterials, Springer, Cham, 2019https://doi.org/10.1007/978-3-319-68255-6_125.

[30] M. Wasim, A. Sabir, M. Shafiq, A. Islam, T. Jamil, Preparation and characterization of composite membrane via layer by layer assembly for desalination, Appl. Surf. Sci. 396 (2017) 259–268, https://doi.org/10.1016/j.apsusc.2016.10.098.

[31] S.V.K.R. Kummari, M.R. Kummara, R.R. Palem, S.R. Nagellea, Y. Shchipunov, C.S. Ha, Chitosan–poly(aminopropyl/phenylsilsesquioxane) hybrid nanocomposite membranes for antibacterial and drug delivery applications, Polym. Int. 64 (2015) 293–302, https://doi.org/10.1002/pi.4789.

[32] G.F. Perotti, J. Tronto, M.A. Bizeto, C.M.S. Izumi, M.L.A. Temperini, A.B. Lugão, D.F. Parra, V.R.L. Constantino, Biopolymer-clay nanocomposites: cassava starch and synthetic clay cast films, J. Braz. Chem. Soc. 25 (2014) 320–330https://doi.org/10.5935/0103-5053.20130300.

[33] H. Alamsi, B. Ghanbarzadeh, A.A. Entezami, Physicochemical properties of starch-CMC-nanoclay biodegradable films, Int. J. Biol. Macromol. 46 (2010) 1–5, https://doi.org/10.1016/j.ijbiomac.2009.10.001.

[34] M. Frydrych, C. Wan, R. Stengler, K.U. O'Kelly, B. Chen, Structure and mechanical properties of gelatin/sepiolite nanocomposite foams, J. Mater. Chem. 21 (2011) 9103–9111, https://doi.org/10.1039/C1JM10788G.

[35] D. Cheikh, R. Martín-Sampedro, H. Majdoub, M. Darder, Alginate bionanocomposite films containing sepiolite modified with polyphenols from myrtle berries extract, Int. J. Biol. Macromol. 165 (2020) 2079–2088, https://doi.org/10.1016/j.ijbiomac.2020.10.052.

[36] M. Darder, M. Lo'pez-Blanco, P. Aranda, A.J. Aznar, J. Bravo, E. Ruiz-Hitzky, Microfibrous chitosan-sepiolite nanocomposites, Chem. Mater. 18 (2006) 1602–1610, https://doi.org/10.1021/cm0523642.

[37] A. Kumar, P. Manju, P.S.G. Krishnan, S.K. Nayak, Physical, mechanical, surface, thermal and morphological studies of PLA-Sepiolite bionanocomposites, J. Miner. Met. Mater. Eng. 3 (2017) 103–111.
[38] E. Ruiz-Hitzky, P. Aranda, A. Alvarez, J. Santaren, A. Esteban-Cubillo, Advanced materials and new applications of Sepiolite and Palygorskite, Dev. Clay Sci. 3 (2011) 393–452, https://doi.org/10.1016/B978-0-444-53607-5.00017-7.
[39] E. Bilotti, H.R. Fischer, T. Peijs, Polymer nanocomposites based on needle-like sepiolite clays: effect of functionalized polymers on the dispersion of nanofiller, crystallinity, and mechanical properties, J. Appl. Polym. Sci. 107 (2008) 1116–1123, https://doi.org/10.1002/app.25395.
[40] D. García-López, J.F. Fernández, J.C. Merino, J. Santarén, J.M. Pastor, Effect of organic modification of sepiolite for PA6 polymer/organoclay nanocomposites, Compos. Sci. Technol. 70 (2010) 1429–1436, https://doi.org/10.1016/j.compscitech.2010.05.020.
[41] N. Saha, R. Shah, P. Gupta, B.B. Mandal, R. Alexandrova, M.D. Sikiricd, P. Saha, PVP - CMC hydrogel: an excellent bioinspired and biocompatible scaffold for osseointegration, Mater. Sci. Eng. C 95 (2019) 440–449, https://doi.org/10.1016/j.msec.2018.04.050.
[42] B. Singha, S. Sharma, A. Dhiman, Acacia gum polysaccharide based hydrogel wound dressings: synthesis, characterization, drug delivery and biomedical properties, Carbohydr. Polym. 165 (2017) 294–303, https://doi.org/10.1016/j.carbpol.2017.02.039.
[43] M. Maswal, O.A. Chat, A.A. Dar, Rheological characterization of multi component hydrogel based on carboxymethyl cellulose: insight into its encapsulation capacity and release kinetics towards ibuprofen, Colloid Polym. Sci. 293 (6) (2015) 1723–1735, https://doi.org/10.1007/s00396-015-3545-4.
[44] J. Cornejo, M.C. Hermosin, Structural alteration of sepiolite by dry grinding, Clay Miner. 23 (4) (1988) 391–398.
[45] C. Wan, B. Chen, Synthesis and characterization of biomimetic hydroxyapatite/ sepiolite nanocomposites, Nanoscale 3 (2) (2011) 693–700, https://doi.org/10.1039/C0NR00650E.
[46] L.H. Gaabour, Effect of selenium oxide nanofiller on the structural, thermal and dielectric properties of CMC/PVP nanocomposites, J Mater Res Technol 9 (2020) 4319–4325, https://doi.org/10.1016/j.jmrt.2020.02.057.
[47] M. Dojcinovic, M. Mitrovic, M. Martic, V. Vucelic, D. Vucelic, Sorption characteristics of paper produced from sepiolite, J.Serb.Chem.Soc. 66 (6) (2001) 385–396, https://doi.org/10.2298/JSC0106385D.
[48] C.O. Plamondon, P. Aranda, A. Favier, G. Habert, H.V. Damme, E.R. Hitzky, The Maya blue nanostructured material concept applied to colouring geopolymers, RSC Adv. 5 (2015) 98834–98841, https://doi.org/10.1039/C5RA14076E.
[49] R.R. Palem, G. Shimoga, K.S.V.K. Rao, S.H. Lee, T.J. Kang, Guar gum graft polymer-based silver nanocomposite hydrogels: synthesis, characterization and its biomedical applications, J. Polym. Res. 27 (3) (2020) 68, https://doi.org/10.1007/s10965-020-2026-8.
[50] Jong-Whan Rhim, Effect of clay contents on mechanical and water vapor barrier properties of agar-based nanocomposite films, Carbohydr. Polym. 86 (2011) 691–699.
[51] A.C.S. Alcântara, M. Darder, P. Aranda, E. Ruiz-Hitzky, Polysaccharide–fibrous clay bionanocomposites, Appl. Clay Sci. 96 (2014) 2–8.
[52] H. Farhadnejad, S.A. Mortazavi, M. Erfan, B. Darbasizadeh, H. Motasadizadeh, Y. Fatahi, Facile preparation and characterization of pH sensitive Mt/CMC nanocomposite hydrogel beads for propranolol controlled release, Int. J. Biol. Macromol. 111 (2018) 696–705, https://doi.org/10.1016/j.ijbiomac.2018.01.061.
[53] B. Giménez, M.C. Gómez-Guillén, M.E. López-Caballero, J. Gómez-Estaca, P. Montero, Role of sepiolite in the release of active compounds from gelatin–egg white films, Food Hydrocoll. 27 (2012) 475–486, https://doi.org/10.1016/j.foodhyd.2011.09.003.
[54] R. Hernandez, S.E.M. Selke, J. Cultler, Plastics Packaging: Properties, Processing, Applications, Regulations, Hanser Gardner Publications, Germany, 2000.
[55] Y.J. Meng, S.Y. Wang, Z.W. Guo, M.M. Cheng, J. Li, D.Q. Li, Design and preparation of quaternized pectin-Montmorillonite hybrid film for sustained drug release, Int. J. Biol. Macromol. 154 (2020) 413–420, https://doi.org/10.1016/j.ijbiomac.2020.03.140.